PHYSICAL REVIEW E VOLUME 61, NUMBER 4 APRIL 2000

Passive particle transport in three-vortex flow

Leonid Kuznetsov[1,*] and George M. Zaslavsky[1,2]
[1]Department of Physics, New York University, 2-4 Washington Place, New York, New York 10003
[2]Courant Institute of Mathematical Sciences, New York University, 251 Mercer Street, New York, New York 10012

(Received 18 June 1999)

We study transport of tracer particles in a two-dimensional incompressible inviscid flow produced by three point vortices of equal strength. Time dependence of the flow caused by vortex motion gives rise to chaotic tracer trajectories, which fill parts of the flow plane referred to as mixing regions. For general vortex positions, a large connected mixing region (chaotic sea) is formed around vortices. It comprises a number of coherent fluid patches (islands), which do not mix with the rest of the chaotic sea, inside them particle motion is predominantly regular; three near-circular islands surrounding vortices are distinguished by their robust nature. Tracers in the chaotic sea rotate around the center of vorticity in an irregular way. Their trajectories are intermittent, long flights of almost regular motion are caused by trappings in the boundary regions of regular islands. The statistics of tracer rotation exhibits anomalous features, such as faster than linear growth of tracer ensemble variance and asymmetric probability distribution with long power tails. Exponent of the variance growth power law is different for different time ranges. Central part of the tracer distribution and its low (noninteger) moments evolve in a self-similar way, characterized by an exponent, which is different from that of the variance, and contrary to the latter is constant in time. Algebraic tails of the tracer distribution, controlling the behavior of the variance, are responsible for this effect. Long correlations in tracer motion lead to non-Poissonian distribution of Poincaré recurrences in the mixing region. Analysis of long recurrences proves, that they are caused by tracer trappings inside boundary layers of islands of regular motion, which always exist inside the mixing region. Statistics of Poincaré recurrences and trapping times exhibit power-law decay, indicating absence of a characteristic relaxation time. Values of the decay exponent for recurrences and for escape from the analyzed traps are very close to each other; long correlations are not dominated by a single trap, but are a cumulative effect of all of them, relative importance of a trap is determined by its size, and by its rotation frequency with respect to the background.

PACS number(s): 47.32.Cc, 05.45.Ac, 05.60.Cd

I. INTRODUCTION

Problem of advection in Lagrangian representation is a problem of finding the pathlines of fluid elements in a prescribed velocity field. It is directly related to the processes of transport of passive particles and passive scalar fields, and has numerous applications in geophysical fluid dynamics, chemical physics, flow visualizations, etc. In many of those, the flow can be considered as two-dimensional and incompressible. In this case, advection is described by a nonautonomous Hamiltonian system, and can be distinguished by the nature of the velocity field of the flow being turbulent, laminar chaotic, regular, or steady. While the last case is rather trivial and leads to particle trajectories coinciding with streamlines of the flow, in the first three cases typical particle path is chaotic, and we have to abandon the idea of tracing individual particle paths and either resort to probabilistic description of advection or seek to find principal dynamical structures governing the character of tracer spreading [1–8].

In this paper, we study transport properties of advection in a flow due to three point vortices moving under their mutual interaction. It can be considered as a continuation of our previous publication [9] on dynamics of tracers in this flow. Velocity field, generated by vortices is a regular, quasiperiodic (periodic in corotating frame) function of time, yet for a generic vortex initial positions some tracer trajectories are chaotic [10,11]. It is a typical example of chaotic advection, which, in a narrow sense, is defined as an appearance of Lagrangian chaos in a regular, fully deterministic velocity field [12]. Chaotic advection deserved a lot of attention for two main reasons: its direct application to transport phenomena in unsteady laminar flows, and as a starting point for the study of large scale transport in two-dimensional turbulence. Point-vortex systems come as a first approximation to the flows dominated by coherent vortical structures, they capture some principal features of such flows [13–16]. Considerable simplification of the flow dynamics allows a detailed analysis of tracer motion in point vortex systems in many cases. When the flow is periodic (in some reference frame), a Poincaré map of tracer trajectories can be used to find regions of chaotic tracer dynamics; such is a situation in oscillating vortex-pair problem [4], three-vortex flow in unbounded plane [11,17,9], leapfrogging motion of two vortex pairs [18], vortex flows is bounded and periodic domains [19–22]. This technique is inapplicable for aperiodic flows; in Ref. [23] particle tracking, tracer cloud spreading, and finite-time Lyapunov exponent analysis were used to study the advection in the field of four chaotically moving point vortices of identical strength, in Ref. [24] similar methods were used for advection in an open chaotic flow due to four vortices with zero total circulation.

---

[*] Present address: Lefschetz Center for Dynamical Systems, Division of Applied Mathematics, Brown University, Providence, RI 02912.

In this paper, we study asymptotic properties of passive particle transport in a flow due to three identical point vortices. The degree of tracer chaotization depends on relative positions of vortices with respect to each other [9]. We look at the most interesting, strongly chaotic case, when vortex motion creates a large connected mixing region in the flow. We have found, that tracer statistics in such flow is anomalous, i.e., non-Gaussian. This result can be related to general properties of transport in Hamiltonian systems [25]. Generic Hamiltonian chaos is not ergodic, the phase space contains an infinite set of islands filled with regular trajectories, forming a fractal structure, which strongly affects the motion in the parts of chaotic sea, adjacent to it. These parts, called singular zones, act as particle quasitraps, and produce long-lasting, algebraically decaying correlations in particle motion [26,27]. The memory effects due to correlations sometimes can be taken into account by the modification of the diffusion coefficient in the Fokker-Plank-Kolmogorov equation [28,29]. However, the influence of correlations if often more profound, leading to nondiffusive kinetics, characterized by nonlinear growth of particle displacement variance in some direction x

$$\sigma^2(t) = \langle (x - \langle x \rangle)^2 \rangle \sim t^{\mu}, \tag{1.1}$$

with non-Gaussian value of the transport exponent $\mu \neq 1$. Such cases are referred to as anomalous diffusion, or, more generally, anomalous transport.

Anomalous transport occurs in many physical settings, both in Hamiltonian and dissipative systems [30–35]. Numerical studies of Hamiltonian flows and maps [36,27,37,38] also provided evidence of non-Gaussian transport, which was named ‘‘strange kinetics’’ [25]. Apart from the nonlinear growth of the variance (1.1), strange kinetics comprises such effects as non-Poissonian distribution of Poincaré recurrences, power-law decay of exit time distributions, etc. A search for a theoretical description of anomalous transport brought up a number of new notions into the field, such as Lévy flights [39], continuous time random walks [40], renewal formalism [41,42], fractional kinetics [43,27,44]. However, despite a considerable progress in our understanding of strange kinetics, some principal questions remain unanswered. Returning to the hydrodynamic language, we may say, that at the present moment there is no complete transport theory of advection, which would be able, for a given velocity field, predict the statistics of tracer dispersion; in other words, given the stream function of the flow $\Psi(x,y,t)$ find the probability distribution function (PDF) for the tracer position $P(x,y,t)$ for large times. For that reason, numerical analysis of the advection statistics remains an important tool in our studies.

In Sec. II, we review the dynamics of the advection in the three point vortex system. Motion of three point vortices is governed by an integrable Hamiltonian system, and is quasiperiodic for almost all values of system parameters (initial conditions). It can be thought of as a superposition of a uniform rotation and periodic relative motion. In a reference frame, corotating with vortices, their motion, and the velocity flow field produced by them, are periodic. Advection equations in the corotating frame have a structure of a periodically forced Hamiltonian system. We analyze the dependence of advection pattern (phase space structure) on the flow parameter, and review some of the analytical results of Ref. [9].

Results of a numerical study of tracer transport properties in the mixing region are presented in Sec. III. Tracer statistics considerably differs from Gaussian, their azimuthal distribution $P(\theta,t)$ has long tails and is asymmetric. Evolution of distribution moments does not follow a single-scaling law, and cannot be described by a unique transport exponent. Recently [45], a notion of strong anomalous diffusion was proposed for a situation of this kind, when the transport exponents are different for small and large moments. In our case, low noninteger moments, obey a relatively simple scaling relationship $M_{\alpha}(t) \sim Ct^{\delta\alpha}$ with exponent $\delta = 0.626$, reflecting a self-similar spreading of the central part of tracer distribution. Higher moments do not obey this scaling, for example, variance ($\alpha = 2$), is characterized by exponent μ (instead of 2δ), which has different values for different time ranges, oscillating between $\mu_1 \approx 1.8$ and $\mu_2 \approx 1.3$.

In Sec. IV, the long-time correlations in tracer motion, leading to the anomalous tracer properties are studied. We start from distribution of Poincaré recurrences to some observation domain inside the mixing region. Short-time recurrences decay exponentially, but do not have a single-characteristic time, due to the existence of a large scale structures in the chaotic sea. Long recurrences have a power-law decay, with the exponent $\gamma \approx 2.6$. Analysis of long Poincaré cycles shows, that they originate from tracer trappings inside singular zones along the borders between regular and chaotic regions. We identify a few principal traps, and build the histograms of residence time distributions for them. Although the sticky zones have very different geometry, their residence time power-law tails have approximately the same value of decay exponent $\gamma_i \approx 2.5$. The exponents in Poincaré recurrence and residence time distributions practically coincide, which is not surprising: it reflects the fact that the majority of long recurrences are due to ‘‘one-trapping’’ cycles. A somewhat faster decay of recurrences can be attributed to the admixture of multiple-trapping events, when a tracer, during its travel between two successive returns to the observation domain, gets stuck inside singular zones more than once.

Since the decay exponents of the major traps are so similar, relative importance of the traps in producing long correlations is determined by the area of singular zones. We have found, that in our system, contributions from several principal traps are comparable, and have to be taken into account when the effects of correlations on transport are studied. As we have mentioned before, these traps are of different origin, i.e., they are not just a family of symmetric islands; a major consequence is that they have different rotation frequencies, in other words, they produce flights with different velocities. This further complicates statistical description of tracer advection: not only a simple Gaussian process, but also a constant velocity Levy-walk model [40], or any other stochastic model assuming constant flight speed, cannot be applied here, without modifications accounting for different flight speeds.

II. ADVECTION DYNAMICS IN THREE-VORTEX FLOW

Trajectory of a passive tracer in an incompressible two-dimensional flow is given by a solution of advection equation, which have a Hamiltonian form

$$\dot{x}=\frac{\partial\Psi(x,y,t)}{\partial y};\quad \dot{y}=-\frac{\partial\Psi(x,y,t)}{\partial x}, \tag{2.1}$$

where x,y are coordinates of the tracer, dot denotes time differentiation, and the flow velocity field is specified by stream function $\Psi(x,y,t)$, so that $\mathbf{v}=(\partial_y\Psi,-\partial_x\Psi)$. Equation (2.1) can be put in a compact form by introducing complex coordinate $z\equiv x+iy$

$$\dot{z}^*=[z^*,\Psi]=2i\frac{\partial\Psi}{\partial z} \tag{2.2}$$

with fundamental Poisson bracket given by $[z,z^*]=-2i$.

Stream function of a system of three point vortices is a sum of contributions of individual vortices [46]

$$\Psi(z,z^*,t)=-\frac{1}{4\pi}\sum_{m=1}^{3}k_m\ln|z-z_m(t)|^2, \tag{2.3}$$

where $z_m(t)\equiv x_m(t)+iy_m(t)$ and k_m are coordinates and strengths of corresponding vortices. The above formula assumes that the flow occupies the whole plane (no walls or other obstacles of the kind) and has zero velocity at infinity. Advection equation takes form

$$\dot{z}^*=[z^*,\Psi]=\frac{1}{2\pi i}\sum_{m=1}^{3}\frac{k_m}{z-z_m(t)}. \tag{2.4}$$

As soon as vortex trajectories $z_m(t)$ are known, the flow is completely specified.

Vortices are advected by mutual interaction. Equation governing their motion is similar to Eq. (2.4)

$$\dot{z}_m^*=\frac{1}{2\pi i}\sum_{j\neq m}\frac{k_j}{z_m-z_j}\quad(m,j=1,2,3), \tag{2.5}$$

where singular self-advection term with $j=m$ should be excluded from the sum. The above system has a number of interesting solutions [47–51], among them finite-time vortex collapse [52] [53], scattering of a vortex pair on a point vortex [54], etc.

We restrict our attention to the vortices of equal strength $k\equiv k_m$, $m=1,2,3$, and discuss relevant features of the solution of Eq. (2.5) for this case, in order to provide an insight at the character of the motion. It was known since Kirchoff, that dynamics of point vortices can be written in the form of Hamilton equations. In case of identical vortices, Eq. (2.5) can be written as

$$\dot{z}_m^*=[z_m^*,H], \tag{2.6}$$

with Hamiltonian function

$$H=-\frac{k}{4\pi}\sum_{j\neq m}\ln|z_m-z_j|^2 \tag{2.7}$$

and fundamental Poisson bracket

$$[z_m,z_j]=0,\quad [z_m,z_j^*]=-2i\delta_{mj}. \tag{2.8}$$

This system is autonomous, and H is an integral of motion. Translational and rotational invariance yield three more first integrals: two components of vortex ''momentum''

$$Q+iP\equiv\sum_{j=1}^{3}kz_j, \tag{2.9}$$

and ''angular momentum''

$$L^2\equiv\sum_{j=1}^{3}k|z_j|^2. \tag{2.10}$$

Out of this four, three integrals in involution can be formed: H, L^2, and Q^2+P^2, which indicates that system (2.6) is integrable. For any vortex configuration, we can introduce a ''center of vorticity'' reference frame by choosing the coordinate system origin at the point $Q+iP$, so that in this coordinates vortex ''momentum'' is zero, i.e., $Q=P=0$. Further, we can rescale coordinates and time

$$z\to z/L,\quad t\to(k/L^2)t. \tag{2.11}$$

Below, we will always use ''center-of-vorticity'' reference frame and dimensionless coordinates (2.11), thus fixing $Q=P=0$, $L=1$, $k=1$. Value of the Hamiltonian H is the only parameter that is left that distinguishes different types of motion. It can be related to the product of side lengths of the vortex triangle Λ

$$e^{-2\pi H}=\Lambda\equiv|z_1-z_2||z_2-z_3||z_3-z_1|. \tag{2.12}$$

Parameter range is from $H=0$, $\Lambda=1$, when vortices stay in the vertices of uniformly rotating equilateral triangle, up to the limiting values $H=\infty$, $\Lambda=0$, when two of the three vortices tend to coalesce. Their is an elegant way [11] to reduce Eq. (2.6) to an equation for ''area variable'' $I(t)$, proportional to the square of the triangle area A

$$I(t)\equiv(16/3)A^2. \tag{2.13}$$

Dynamics of $I(t)$ is given by

$$\left(\frac{dI}{d\tau}\right)^2=-I[I^3+6I^2+3(3-8\Lambda^2)I+8\Lambda^2(2\Lambda^2-1)]$$
$$\equiv-P(I;\Lambda), \tag{2.14}$$

where $\tau=3/(2\pi\Lambda^2)t$. It can be thought of as a motion of a particle of mass 2 with zero total energy in the potential $P(I;\Lambda)$. This motion can be of three different types: for Λ less, equal or larger than $\Lambda_c\equiv1/\sqrt{2}$. Shape of the potential well for these three cases is shown in Fig. 1. When $\Lambda<\Lambda_c$, $I(t)$ reaches zero periodically, i.e., vortices periodically pass through an aligned configuration; for $\Lambda=\Lambda_c$ motion is aperiodic, aligned configuration turns into an unstable equilibrium; and for $\Lambda>\Lambda_c$ $I(t)$ oscillates between two positive roots of $P(I;\Lambda)$—vortices never get aligned. Solution of Eq. (2.14) can be written in terms of Jacobi elliptic functions [11] [9], it is periodic for $\Lambda\neq\Lambda_c$, with period $T(\Lambda)$ diverging logarithmically as $\Lambda\to\Lambda_c$. Vortex trajectories can be reconstructed from $I(t)$, they are given by

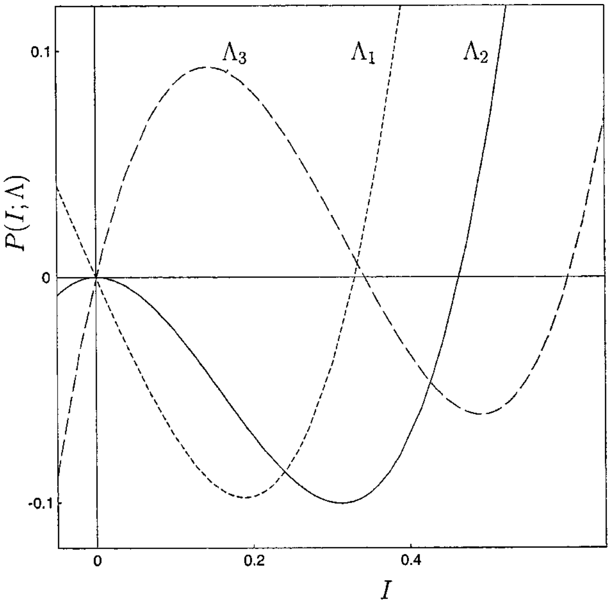

FIG. 1. Effective potential $P(I;\Lambda)$ for the dynamics of the area variable $I(\tau)$, shown for three values of Λ: $\Lambda_1=0.6<\Lambda_c$; $\Lambda_1=1/\sqrt{2}=\Lambda_c$; $\Lambda_1=0.8>\Lambda_c$.

$$z_m(t)=6^{-1/2}Le^{i\phi_2(t)/2}\{[1-I^{1/2}(t)]^{1/2}e^{-2\pi i(m-1)/3}e^{-i\phi_1(t)/2}+[1+I^{1/2}(t)]^{1/2}e^{-4\pi i(m-1)/3}e^{i\phi_1(t)/2}\},\quad (m=1,2,3)\tag{2.15}$$

where "configuration angle" $\phi_1(t)$ is defined by

$$\cos 3\phi_1=\frac{(1+3I)-4\Lambda^2}{(1-I)^{3/2}}\tag{2.16}$$

and "rotation angle" $\phi_2(t)$ can be written as a quadrature of some function of $I(t)$ [9]. Note that relative motion of vortices, described by the term in square brackets in Eq. (2.15) is periodic [47,11] (with period $T_{\text{rel}}=2T$ for $\Lambda<\Lambda_c$ and $T_{\text{rel}}=3T$ for $\Lambda>\Lambda_c$), and during each period the whole configuration is rotated by a constant angle $\Theta(\Lambda)\equiv\phi_2(T_{\text{rel}})-\phi_2(0)$, which means we can consider vortex motion as a superposition of periodic motion and rotation with constant angular velocity [17,9]

$$\Omega(\Lambda)\equiv\Theta(\Lambda)/T_{\text{rel}}.\tag{2.17}$$

In general, $\Omega(\Lambda)$ is incommensurate with 2π, and vortex trajectories $z_m(t)$ are quasiperiodic.

In addition to the laboratory "center of vorticity" reference frame, defined above, it is convenient to consider another reference frame, corotating with vortices with angular velocity $\Omega(\Lambda)$. Vortex trajectories in the corotating frame

$$\tilde{z}_m(t)=z_m(t)e^{-i\Omega(\Lambda)t},\quad m=1,2,3\tag{2.18}$$

are periodic with period T_{rel}. The advection Eq. (2.4) in the corotating frame takes form

$$\dot{\tilde{z}}^*=[\tilde{z}^*,\tilde{\Psi}]=\frac{k}{2\pi i}\sum_{m=1}^{3}\frac{1}{\tilde{z}-\tilde{z}_m(t)}+i\Omega(\Lambda)\tilde{z}^*,\tag{2.19}$$

where $\tilde{z}=ze^{-i\Omega t}$ is tracer coordinate in the corotating frame, and the stream function (periodic in time with period T) acquires an additional term, corresponding to rotational "energy"

$$\tilde{\Psi}(\tilde{z},\tilde{z}^*,t)=-\frac{k}{4\pi}\sum_{j=1}^{3}\ln|\tilde{z}-\tilde{z}_j(t)|^2+\frac{\Omega(\Lambda)}{2}\tilde{z}\tilde{z}^*.\tag{2.20}$$

System (2.19) belongs to the class of Hamiltonian systems with $1\frac{1}{2}$ degrees of freedom, its solutions can be regular or chaotic, depending on the initial position of the tracer, and the character of vortex motion, i.e., form of functions $\tilde{z}_m(t)$ specified by Λ. Appearance of chaotic tracer trajectories in this system was first demonstrated in Refs. [11] and [10]. Structure of the advection pattern, i.e., dependence of the solution type on the initial position, was analyzed numerically in Ref. [17] and numerically and analytically in Ref. [9].

Below we present examples of advection patterns for four values of the parameter Λ, illustrating the variety of phase space structures in three-vortex flow. Periodicity of the flow in the corotating frame allows to construct Poincaré map of tracer trajectories. We integrate Eq. (2.4) numerically and record tracer position (in the corotating frame) with time interval equal to the period of the flow T, see Fig. 2. It turns out, that degree of chaotization of tracer motion varies considerably with the change of the geometry of the background vortex motion. When $\Lambda=1$, vortices do not move in the corotating frame and Eq. (2.19) becomes an autonomous system, so advection is integrable—tracers move along the level curves of Eq. (2.20) (streamlines). Among those, there are two sets of separatrices, connecting saddle points of $\tilde{\Psi}(\tilde{z},\tilde{z}^*)$, where tracer trajectory is aperiodic. They are the seeds of chaos—even for the slightly distorted equilateral configuration with $\Lambda=1-\epsilon$, $\epsilon\ll 1$, when vortices start to oscillate around the equilibrium position with amplitude of order $\sqrt{\epsilon}$, the separatrices split and form two thin mixing layers, Fig. 2(a). These layers merge together for fairly small value of distortion $\epsilon\approx 10^{-6}$, mixing region grows very fast as Λ decreases, see Fig. 2(b), $\Lambda=0.94$. The strongest chaotization occurs when Λ is close to Λ_c, Fig. 2(c). After Λ passes its critical value Λ_c, the type of vortex motion changes. This is reflected in the change of the symmetry of vortex trajectories: in "triangular" regime, $\Lambda>\Lambda_c$, all three vortex trajectories can be obtained from each other

$$\tilde{z}_m(t+T_{\text{rel}}/3)=\tilde{z}_j(t)e^{2\pi i/3},\quad m=1,2,3;\quad j-1=m \bmod 3.\tag{2.21}$$

In the "two plus one" case, $\Lambda<\Lambda_c$, the vortex that was initially further from the other two becomes special—it keeps oscillating in its own corner, while the other two change places with each other. There is still a symmetry

$$\tilde{z}_2(t+T_{\text{rel}}/2)=\tilde{z}_3(t);\quad \tilde{z}_3(t+T_{\text{rel}}/2)=\tilde{z}_2(t);$$
$$\tilde{z}_1(t+T_{\text{rel}}/2)=\tilde{z}_1(t),\tag{2.22}$$

but it is only between $\tilde{z}_2$ and $\tilde{z}_3$ (two vortices in the bottom in Fig. 2). These symmetries explain the relation between the period of vortex trajectories T_{rel} and the period of the stream

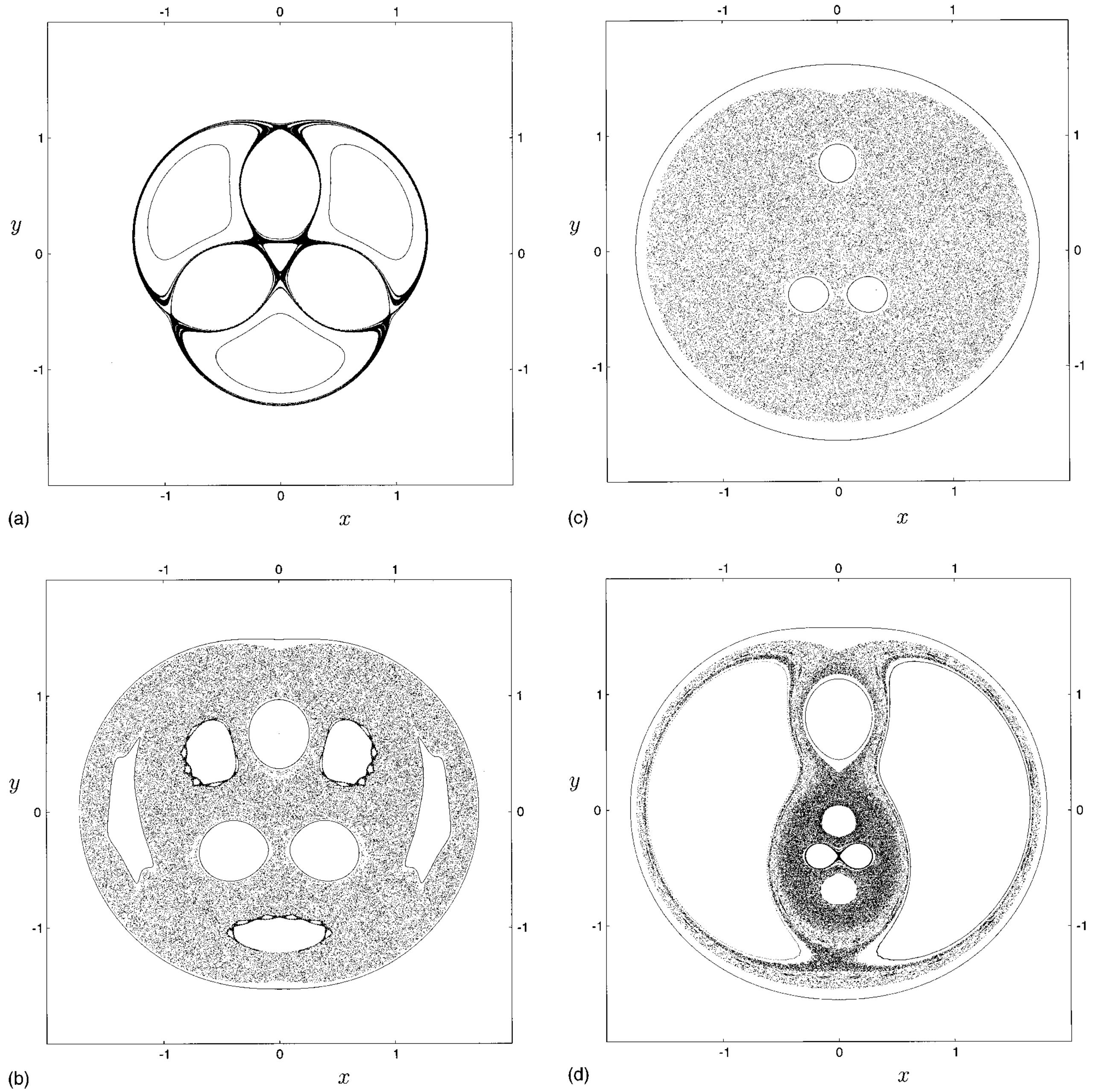

FIG. 2. Advection patterns for different vortex geometries: (a) Weak chaos, $\Lambda = 1 - 2.4\times 10^{-7}$; (b) $\Lambda = 0.94$; two types of islands in the chaotic sea: three smooth vortex cores and elliptic islands with rugged boundaries. (c) $\Lambda = 0.707109$; strong chaos, elliptic islands vanish from sight (very small islands still can be detected). Vortex cores are robust. (d) $\Lambda = 0.464$; as Λ gets smaller, the advection pattern starts to resemble that of a two-vortex system.

function *T*. As Λ gets smaller, the asymmetry between the isolated vortex and vortices forming a pair becomes more pronounced—the coherent core around the former grows, while the cores of the pair gets smaller, Fig. 2(d). Mixing region shrinks, and as $\Lambda \to 0$ the advection pattern approaches more and more to the regular advection in the field of two point vortices with strengths k and $2k$.

Except for the near-integrable cases $\Lambda \approx 1$ and $\Lambda \ll 1$, the advection pattern has three main types of components: (i) ‘‘far region,’’ where tracer motion is regular, roughly occupying the outside of the circle of radius $R_{\max} \approx 1.6$; (ii) mixing region inside this circle where fluid is efficiently stirred by vortex motion; (ii) islands of regular motion inside the mixing region, which are of two different types: three smooth, robust, near-circular patches surrounding vortices and moving together with them, forming coherent structures known as *vortex cores*, and elliptic islands, surrounding stable periodic orbits, number of which, as well as their size and shape, depends in a very sensitive manner on the smallest variations in the background flow. In Ref. [9] the robust nature of the vortex cores was explained and expressions for their radius ζ_c and for radius of the external boundary of the mixing region $R_{\max}$ as function of the background flow geometry were derived. For small deviations $\delta\Lambda \equiv \Lambda - \Lambda_c$ from critical configuration, the core radius is given by

$$\zeta_c = \left[\frac{\pi\sqrt{3}}{18(\ln\ln|\delta\Lambda|^{-1} + \ln 4C_2)} \right]^{1/2}, \tag{2.23}$$

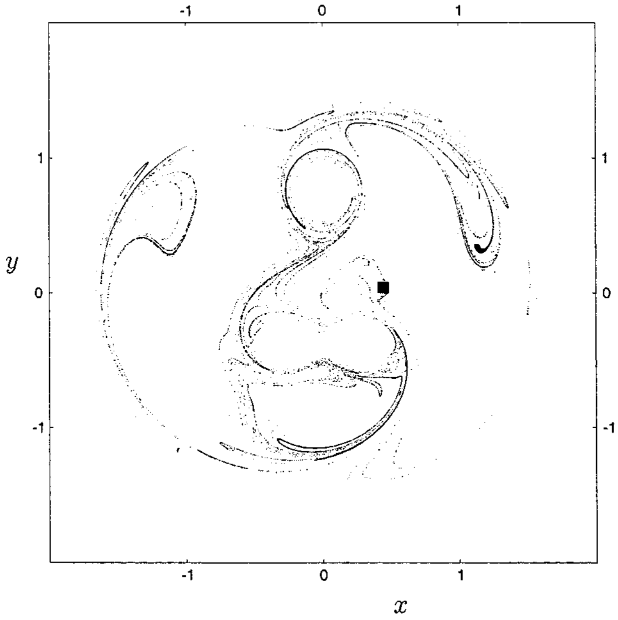

FIG. 3. Tracer mixing. Originally concentrated in a rectangle at (0.5, 0), after only two periods of vortex motion tracers are spread around the chaotic sea. Manifold structures still can be seen.

where constant $C_2=74.3$ for nonisolated vortex position (all three vortices for $\Lambda>\Lambda_c$ and vortices in the pair for $\Lambda<\Lambda_c$), and $C_2=1.20$ for isolated vortex in case $\Lambda<\Lambda_c$. The outside radius of the mixing region is

$$R_{\max}=\left(\frac{8B\ln|\delta\Lambda|}{3\sqrt{3}}\right)^{1/6}, \tag{2.24}$$

where constant $B=0.41$ for both cases $\Lambda>\Lambda_c$ and $\Lambda<\Lambda_c$.

The tracer motion in regular regions is quasiperiodic, and can be studied in as much detail as necessary by direct dynamical analysis. For example, tracer trajectories in the far region, or inside the cores can be found using perturbation theory up to the desirable degree of approximation [9]. This procedure may get technically complicated, especially for the motion inside elliptic islands of higher generations, but the big picture is essentially the same—the island as a whole moves quasiperiodically inside the chaotic sea, with all the tracers inside trapped forever. We should mention, that strictly speaking, some of the inside tracers move chaotically, since the Kol'mogorov-Arnol'd-Moser (KAM) tori of regular motion are interlayered with thin stochastic layers (in place of destroyed resonances). This generic property has certain principal consequences, in particular it negates a possibility of determining the motion inside the regular regions *exactly*, but it is not relevant on bigger scales.

III. STATISTICS OF ANGULAR ADVECTION

In the mixing region one cannot follow individual tracer trajectories for longer than a few periods of vortex motion, they diverge exponentially and spread over the whole chaotic sea, Fig. 3. The key features of the dynamics of this process can be understood in terms of the evolution of the hyperbolic points and their invariant manifolds, which govern the geometry of mixing, i.e., the way fluid elements are stretched and folded. However, to extract a long-term statistics of the tracer motion from the manifold geometry can be a prohibitively difficult task. The reason for that is the crucial influence of the fine structures in the chaotic sea, such as hierarchies of island chains, that, although very small, cannot be neglected because they introduce long-time correlations, and cause intermittent behavior of the tracer trajectories.

Alternative approach is to model the motion in the chaotic sea as a random process. A central problem here is how to specify, for a given velocity field, the type and parameters of this random process. A major difficulty is the sensitivity of the long-term tracer statistics on the small variations in the control parameters of the flow, arising from the sensitivity of the fine topological structures in the chaotic sea. Despite a considerable progress in the understanding of the origin of the long-time correlations, created by the stickiness of the trajectories to the singular zones surrounding regular islands, and of their influence on the statistics, one still have to rely on numerical simulations in order to construct a realistic approximation for the transport in the mixing region.

To study statistics of the tracer motion, we have numerically integrated equations for the tracer trajectories (2.4), for a typical case of strongly mixing background vortex flow with $\Lambda=0.717$. Advection pattern for this value of the flow parameter exhibits different types of interesting phase space structures: vortex cores with sticky bands on their borders, elliptic islands with different kinds of boundary chains, and sticky outer rim of the chaotic region. We use a fifth-order symplectic Gauss-Legendre scheme [55] with a time step $\Delta t=0.04$, such that $v_{\max}\Delta t\approx 0.03$, where $v_{\max}\approx(2\pi\zeta_c)^{-2}\approx 0.78$ is the fastest frequency of the problem, determined by the closest approach of the tracer to the vortex $\zeta_c\approx 0.18$. Symplectic schemes are a natural choice for numerical integration of Hamiltonian systems, in particular, for the case of a four-point vortex system they work better than standard Runge-Kutta schemes [56], although recently in Ref. [23] it was demonstrated, that higher order adaptive Runge-Kutta schemes can yield similar performance.

Poincaré sections of tracer trajectories, shown in Fig. 4 for different phases ($t=0,T/4,T/2,3T/4$) of vortex configuration, illustrate the dynamics of the advection pattern, and allow to express the rotation frequencies of the regular islands, through the frequency of corotating frame $\nu_{\mathrm{rot}}\equiv\Omega/(2\pi)=0.0879$ and the frequency of vortex relative motion $\nu_{\mathrm{rel}}\equiv 1/T_{\mathrm{rel}}=0.0511$.

Let us concentrate our attention on the angular advection of tracers, since their motion in the radial direction is bounded by the outer border of the mixing region (2.24). To describe the angular motion of a tracer, let us consider its azimuthal coordinate

$$\theta(t)\equiv \operatorname{Arg} z \tag{3.1}$$

as a continuous function of time, in other words, $\theta(t)$ is not confined to the interval $(0;2\pi)$, but keeps track of the number of whole rotations performed by a tracer since the beginning of its motion. We start with an ensemble of 6144 tracers and numerically integrate their trajectories for $t_{\max}=512000$ time units [see Eq. (2.11) for definition of the time scale] which corresponds to $N_{\max}\approx 26160$ periods of vortex relative motion. All initial conditions were taken inside the mixing re-

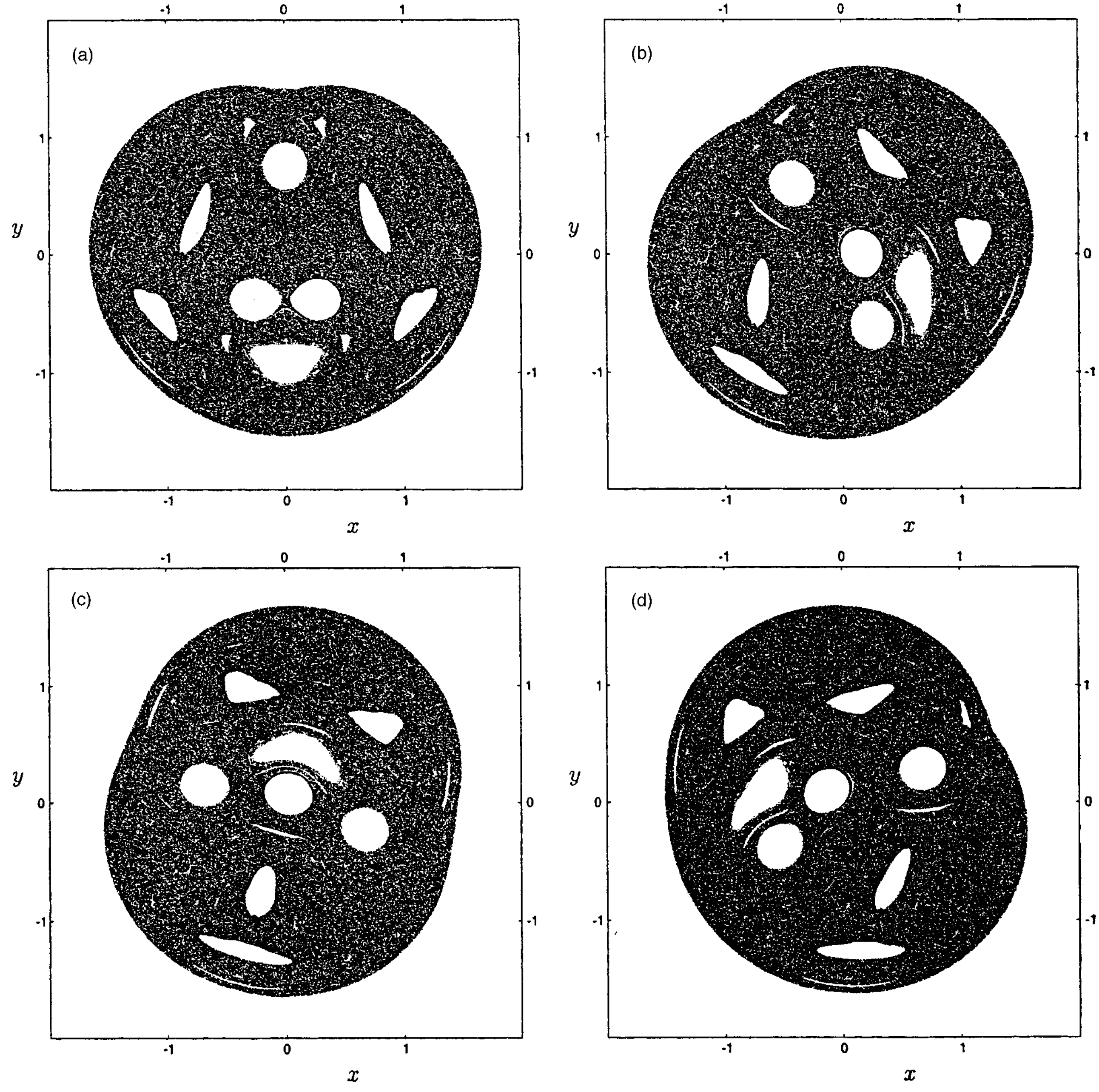

FIG. 4. Advection pattern for different phases of vortex configuration. (a) Configuration with maximum of the vortex triangle area corresponds to $t=0$; (b) quarter of the area oscillation period: $t=T/4$; (c) half-period: $t=T/2$; (d) $t=3T/4$.

gion. Mean advection angle $\langle\theta(t)\rangle$ and the angular variance $\sigma^2(t)\equiv\langle[\theta(t)-\langle\theta(t)\rangle]^2\rangle$ are defined as averages over the ensemble. Typical evolution of tracer azimuth is illustrated by Fig. 5, where $\theta(t)-\langle\theta(t)\rangle$ is plotted for eight trajectories. Intermittent character of tracer motion is clearly seen, apparently random pieces of trajectory are interrupted by regular flights, some of which are quite long.

The mean grows linearly with time (except for the very beginning of the motion) and we can define an average rotation frequency for the chaotic sea

$$\overline{\nu}\equiv\langle\theta(t)\rangle/(2\pi t), \tag{3.2}$$

its value is $\overline{\nu}\approx 0.0742$. The growth of the variance is not linear. Figure 6(a) shows the log-log plot of the variance versus time, indicating the anomalous character of the angular diffusion. Moreover, different time ranges have different transport exponents

$$\begin{aligned} t<10^4 \quad & \sigma^2(t)\sim t^{\mu_1} \quad \mu_1\approx 1.79 \\ 10^4<t<10^6 \quad & \sigma^2(t)\sim t^{\mu_2} \quad \mu_2\approx 1.32 \\ t>10^6 \quad & \sigma^2(t)\sim t^{\mu_3} \quad \mu_3\approx 1.78 \end{aligned} \tag{3.3}$$

as can be seen from Fig. 6(a). This behavior of the variance can be explained by the so-called log-periodic oscillations [57], which infer existence of a discrete renormalization property of trajectories, when they stick to a hierarchical chains of islands.

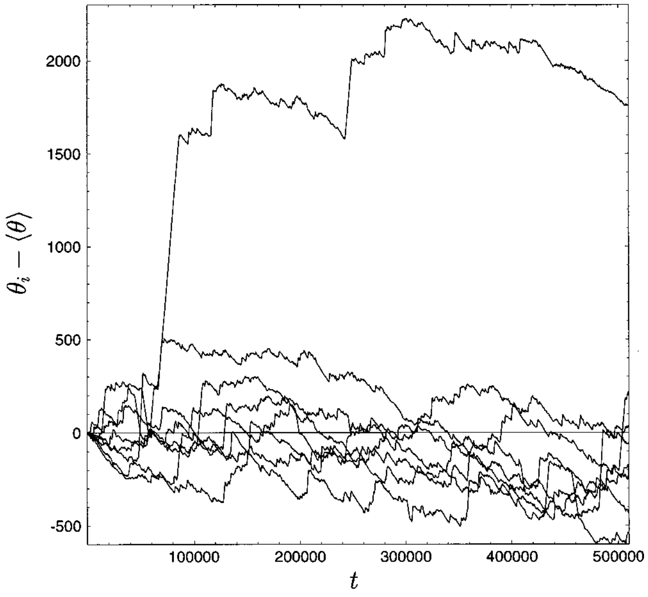

FIG. 5. Time series of the azimuthal coordinate $\theta-\langle\theta\rangle$ for eight typical tracer trajectories.

To detect a source of this behavior, we look at the form and the evolution of the angular probability density function of the tracers $P(\theta;t)$, which is constructed by building a histogram of a numerically obtained set of values of $\theta(t)$ of the tracer ensemble for a given time.

For many stochastic processes, PDF at large times evolves in a self-similar way

$$P(X;t)=g(t)f(\xi) \quad \xi\equiv g(t)[X-\langle X\rangle]. \tag{3.4}$$

For example, PDF of a Gaussian random variable X has

$$P(X;t)=(\pi t)^{-1/2}\exp\xi^2/2 \quad \xi\equiv t^{-1/2}[X-\langle X\rangle] \tag{3.5}$$

and a PDF of a Levy-type process (random walker with infinite mean-square step length)

$$P(X;t)=t^{-1/\delta}f(\xi) \quad \xi\equiv t^{-1/\delta}X. \tag{3.6}$$

To check if the obtained PDF of tracer rotation angles evolves in such self-similar way, we have looked at the time dependence of the probability density at the center of distribution, $P_{\max}(t)=P(\langle\theta\rangle;t)$. It turns out, that $P_{\max}(t)$ quite accurately follows a power law $P_{\max}(t)\sim t^{-\delta}$ with an exponent $\delta\approx 0.626$, which suggests that PDF may have a form

$$P(\theta,t)=t^{-\delta}f(\xi), \quad \xi=[\theta(t)-\langle\theta(t)\rangle]t^{-\delta}. \tag{3.7}$$

Indeed, plots of tracer PDF as function of ξ for different times coincide, see Fig. 6(b) indicating that self similarity (3.7) does hold.

There is a seeming discrepancy between this result and the behavior of the variance (3.3). According to Eq. (3.7), the time dependence of the nth moment is given by

$$M_n(t)=\int \theta^n P(\theta,t)d\theta = t^{\delta n}\int \xi^n f(\xi)d\xi \sim Ct^{\delta n} \tag{3.8}$$

and the variance have to grow as $\sigma^2(t)\sim t^{2\delta}$, so that the value of the transport exponent should be constant: $\mu=2\delta\approx 1.25$. However, Eq. (3.8) holds only if $f(\xi)$ decays fast enough at infinity. If $f(\xi)$ has a power tail, $f(\xi)\sim\xi^{-\eta}$, only the moments with $n<\eta-1$ will follow Eq. (3.8), whereas higher moments are determined by the cutoff of the distribution at large θ. Tails of the tracer PDF, plotted in Fig. 6(c) for four different times indicate a decay according to a power law

$$P(\theta;t)\sim(\theta-\langle\theta\rangle)^{-\eta} \tag{3.9}$$

with $\eta=2.72$. For such slow decay, all moments starting from the variance ($n=2$) are defined by the far end of the distribution, i.e., by a specific mechanism of the cutoff at large θ.

Self similarity (3.7) and (3.8) can be traced in the behavior of the noninteger moments $M_\alpha(t)=\int\theta^\alpha P(\theta,t)d\theta$ for $\alpha<\eta-1$, which are defined by the central part of the distribution (Fig. 7). We have a situation, when a unique exponent is not enough to completely characterize anomalous behavior of tracer transport. This case was named *strong anomalous diffusion* in Ref. [45], in contrast to the case of weak anomalous diffusion, when the evolution of all moments is described by a single exponent δ, according to Eq. (3.8).

The origin of the power tails of $P(\theta,t)$ as well as of the other anomalous properties of the tracer statistics, lies in the intermittent character of the tracer motion in the mixing region, caused by tracer trappings in the singular zones, surrounding KAM islands. A piece of a chaotic tracer trajectory, during which the tracer is caught in the hierarchical structure at the island border is almost regular—the tracer is carried along with the island in a ballistic flight, characterized by almost constant angular velocity (averaged over times of order T). Appearance of flights and their dominant role in particle statistics is typical for the chaotic flows [58,36].

The structure of the singular zones on the island borders is usually very sensitive to the variations of the parameters of the flow. In some situations, particle quasi-traps can vanish altogether from the chaotic sea, resulting in the ''restoration'' of the normal diffusive behavior [58]. We have looked for such situation for a three-vortex flow, trying to find a value of the parameter Λ for which tracer statistics becomes Gaussian at large times. The results of this search were negative, but insightful. Taking a value of Λ, for which the advection pattern is seemingly devoid of sticky structures [Fig. 2(c)], we have propagated an ensemble of particles in this flow, looking at the behavior of the variance $\sigma^2(t)$. If the number of the particles in the ensemble is not too large, the resulting angular diffusion appears normal: $\sigma^2(t)\sim t$. However, after the ensemble size is increased, some of the tracers fall into small quasitraps hidden in the chaotic sea and long flights appear, destroying Gaussian statistics.

IV. POINCARÉ RECURRENCES AND FLIGHTS

Poincaré map of the tracer trajectories used in Sec. II to visualize advection patterns, can be employed to study correlations in the tracer motion. When a tracer is moving in a flight, its trajectory is localized around a particular trap in the phase space, so that during the time of the flight it does not visit the well-mixed component of the stochastic sea. If we take a domain B in the well-mixed region, and examine Poincaré recurrences to B, a flight will indicate itself by produc-

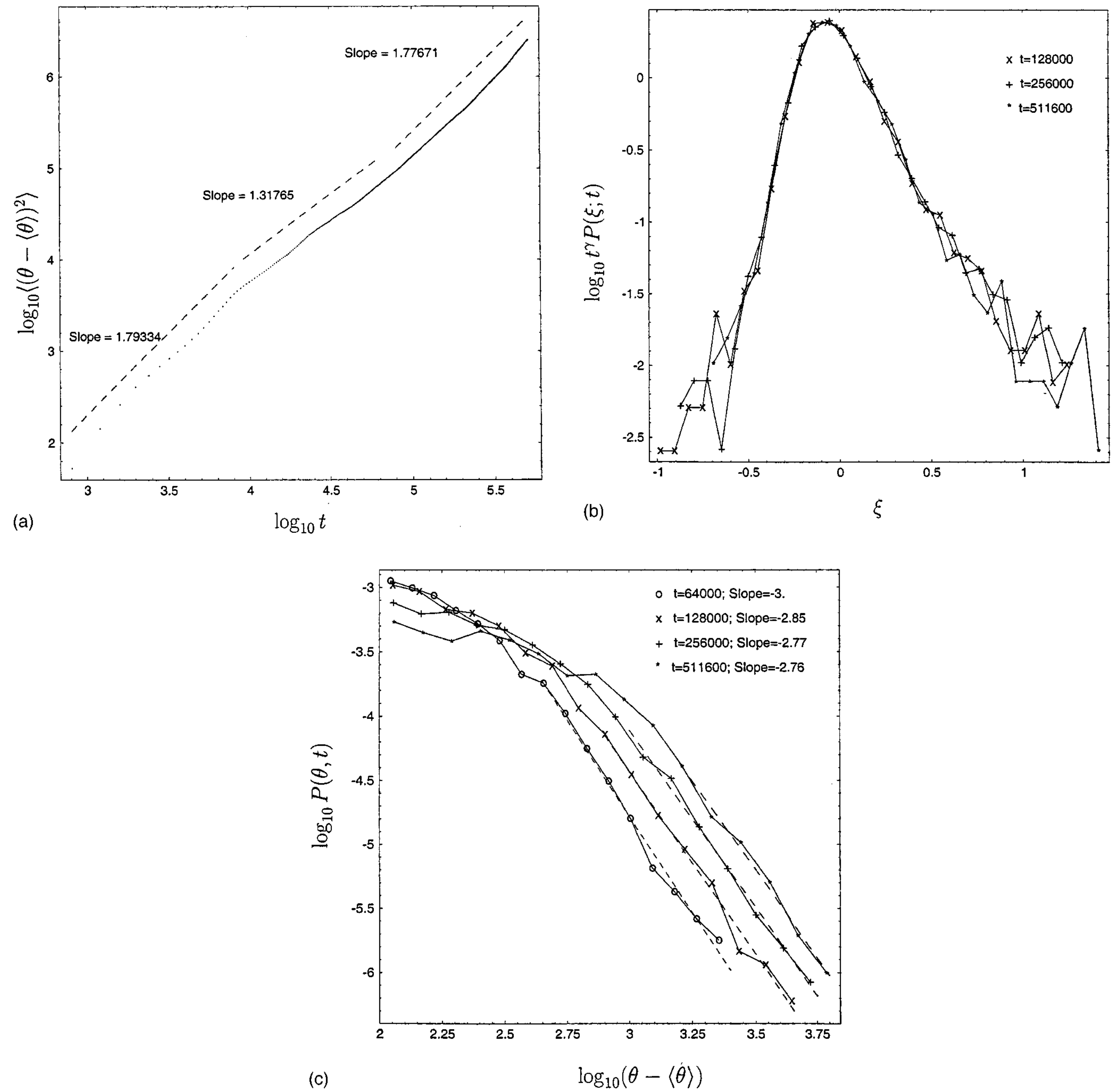

FIG. 6. (a) Anomalous growth of tracer ensemble variance: $\sigma^2(t) \sim t^{\mu}$. Transport exponent μ is different for different time ranges, see Eq. (3.3). (b) Scaled probability density of tracer angular displacement (3.7) as a function of the similarity variable $\xi \equiv t^{-\delta}(\theta - \langle\theta\rangle)$, $\delta = 0.625$. (c) Tails (not scaled) of the same distribution in log-log scale show a slow, power-law decay with exponent $\eta \approx 2.8$.

ing a long-recurrent event. Analysis of such events can reveal what flight types are present in a system, and determine characteristics for each type of flights, e.g., flight velocity (angular frequency in our geometry), domains of localization, flight length PDF, etc.

In this section, we will analyze tracer flights in a three-vortex flow with $\Lambda = 0.717$, following the above recipe. To start, we need to chose a box B in the well-mixed region of the flow. We cannot take it very large, because we want all quasitraps to be outside of B, in order to be able to detect them. On the other hand, we cannot take it very small either, since in that case flights will be shadowed by a background of random, no-flight recurrences.

Indeed, the PDF of the recurrence time $P(\tau;B)$ can be thought of as a sum of contributions from long-correlated flights $P_{fl}(\tau;B)$ and from recurrences due to random motion in the well-mixed region $P_{\mathrm{mix}}(\tau;B)$:

$$P(\tau;B) = \begin{cases} P_{\mathrm{mix}}(\tau;B), & \text{if } \tau < \tau_c \\ P_{fl}(\tau;B), & \text{if } \tau > \tau_c, \end{cases} \tag{4.1}$$

where τ_c is a crossover time. We expect that the distribution of random recurrences resembles a Poissonian distribution, typical for the dynamical chaos with perfect mixing (see Refs. [27] and [59] and references therein)

$$P_{\mathrm{mix}}(\tau;B) = [1/\langle\tau'\rangle] e^{-\tau/\langle\tau'\rangle}. \tag{4.2}$$

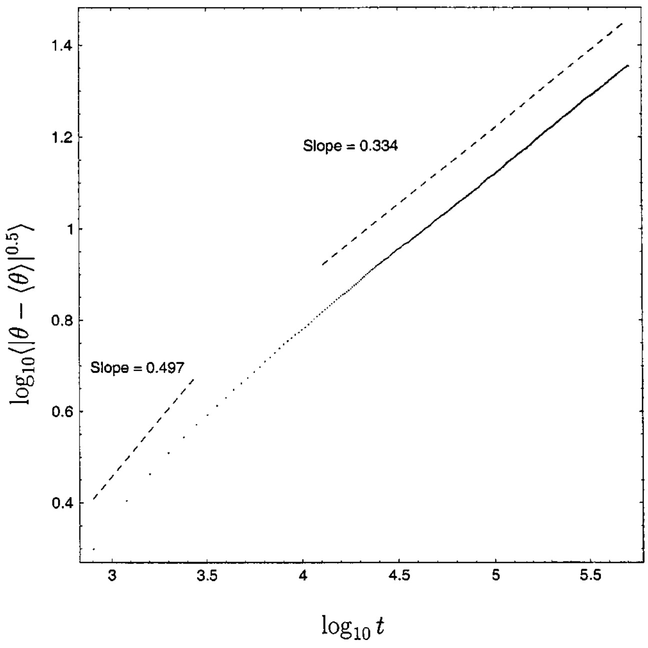

FIG. 7. Growth of noninteger moment $M_{0.5}\sim t^{\delta/2}$ is consistent with the self-similarity (3.7) of the central part of tracer distribution.

In this situation recurrences longer than $\langle\tau'\rangle$ are practically solely due to flights, whereas those of order $\langle\tau'\rangle$ and shorter are predominantly of random origin. Maximum observable flight length is restricted by the total integration time $t_{\max}$, so the flight tail of the recurrences distribution is limited to the middle part of the interval $(\langle\tau'\rangle, t_{\max})$. In our system, traps occupy a relatively small portion of the chaotic sea, and flight events are rare, in a sense that mean recurrence time for no-flight events $\langle\tau'\rangle$ is of the same order as the total mean recurrence time

$$\langle\tau\rangle \equiv \int_0^\infty \tau P(\tau;B)\, d\tau. \tag{4.3}$$

Since we assume motion in the chaotic region to be ergodic, $\langle\tau\rangle$ should be inversely proportional to the area of the observation domain B

$$\langle\tau\rangle = (\Gamma_0/B) T_{\mathrm{rel}}, \tag{4.4}$$

where Γ_0 is admissible volume [60,61]. If we take B too small, $\langle\tau\rangle$ and $\langle\tau'\rangle$ can get comparable with $t_{\max}$, and there will be no flight tail to analyze, PDF of the Poincaré recurrences (4.1) will be dominated by random events for all observation period $t<t_{\max}$.

Poincaré map we are using is defined as follows. For a point z_0 in the *corotating* advection plane, let us denote $z(t;z_0)$ a tracer trajectory originating at z_0, i.e., a solution of Eq. (2.19) with initial condition $z(0;z_0)=z_0$. Then, an image of z_0 is given by a position of the tracer after one period of relative vortex motion T_{rel}

$$\hat{M}(z_0) = z(T_{\mathrm{rel}};z_0). \tag{4.5}$$

The map $\hat{M}$ depends on the choice of Poincaré section plane, specified by a vortex phase at $t=0$. We chose to set $t=0$ at the moment when vortices form an isosceles triangle with all acute angles (the vortex triangle area reaches its maximum), see Fig. 4(a).

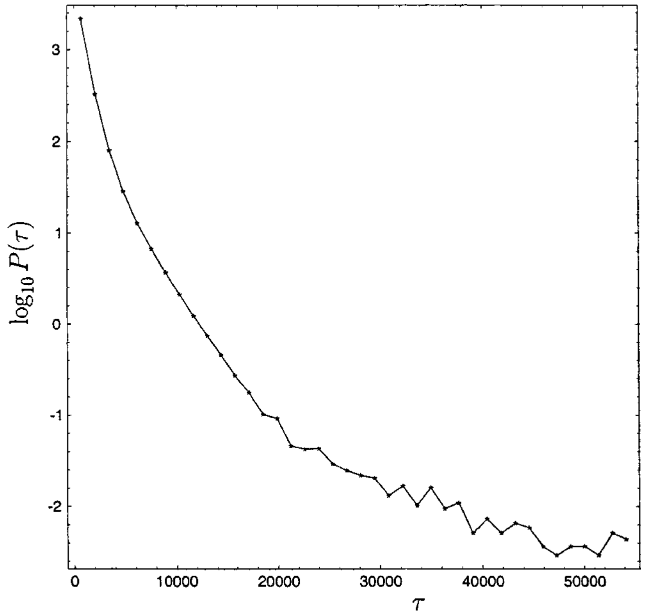

FIG. 8. Distribution of Poincaré recurrences to the box B: $x\in(0,0.4)$, $y\in(0,0.4)$.

As an observation domain B, we took a square B: $x\in(0,0.4)$, $y\in(0,0.4)$ in the well-mixed part of the stochastic sea. To collect recurrence statistics the same ensemble of $N=6144$ tracer trajectories integrated till $t_{\max}=512000$ time units (2.11) as in Sec. III was used. Each tracer trajectory generates a corresponding trajectory of the map $\hat{M}$—a sequence $\{z_n = z(nT_{\mathrm{rel}})\}$ with n running from zero to $N_{\max} = t_{\max}/T_{\mathrm{rel}} \approx 26160$. We define return times a as a subsequence of map times $\{nT_{\mathrm{rel}}\}$ corresponding to return events: $\{t_i = n_i T_{\mathrm{rel}}:\ z_{n_i}\in B,\ z_{n_i-1}\notin B\}$, and recurrence times as intervals between successive returns: $\{\tau_i = t_i - t_{i-1}\}$.

A histogram of the distribution of Poincaré recurrences $P(\tau)$ to the box B is shown in Fig. 8. The total number of recurrences, generated by our tracer ensemble was $N_{\mathrm{rec}} = 3{,}607{,}086$; the longest recurrence time was $\tau_{\max} = 355{,}899$; which is comparable with total integration time $t_{\max}$. For small τ, $P(\tau)$ decays exponentially, although the decay rate changes from $\langle\tau_1'\rangle \approx 670$ to $\langle\tau_2'\rangle \approx 2800$ when τ goes from 10^2 to 10^4 (see Fig. 8). This indicates a presence of permeable barriers (cantori), separating the mixing region into several parts of comparable areas. Particles returning to B without crossing these barriers have shorter characteristic return time, that the ones crossing it. Mean recurrence time (4.3) is $\langle\tau\rangle \approx 850$, it is of order $\langle\tau_1'\rangle$—fast recurrences dominate. Its knowledge allows us to find the total area of the mixing region (excluding islands), using Eq. (4.4) we get $\Gamma_0 = (\langle\tau\rangle/T_{\mathrm{rel}})\ B = 6.9$ (compare to Fig. 4). Crossover from exponential to algebraic decay occurs at $\tau_c \approx 2\times10^4$. As an experimental argument in favor of choosing large observation domain, we compare the tails of distributions of Poincaré recurrences to the box B and to the smaller box B_2: $x\in(0,0.2)$, $y\in(0,0.2)$ [Fig. 9(a)]. Both distributions are obtained from the same set of trajectories, so they are supposed to capture the same amount of long-correlated flights. In the

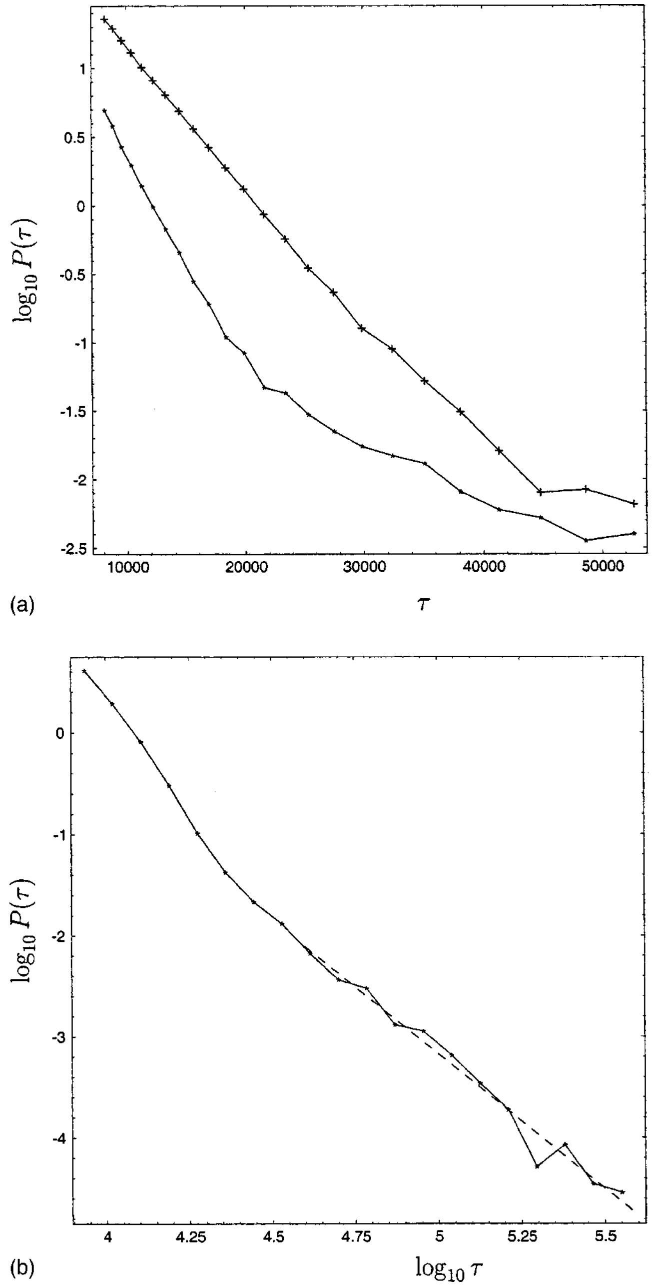

FIG. 9. (a) Comparison of the tails of Poincaré recurrences to the box B: $x \in (0,0.4)$, $y \in (0,0.4)$, with that to the smaller box B_2: $x \in (0,0.2)$, $y \in (0,0.2)$; bigger box is more effective in separating flight tails from the background of random recurrences. (b) Tail of Poincaré recurrences to B in log-log scale exhibits a power-law decay, with the exponent $\gamma \approx 2.66$, see Eqs. (4.6) and (4.7).

latter case (box B_2) a crossover to power law starts only at $\tau_{c_2} \approx 45\,000$, which means, that flights with duration less that τ_{c_2} are shadowed by random recurrences, i.e., lost.

Our main object of interest is long recurrences, ones bringing in the anomalous transport properties. The tail of the distribution, plotted in Fig. 9(b) in log-log scale, shows a power-law decay at large τ

$$P(\tau) \sim \tau^{-\gamma} \tag{4.6}$$

with the exponent

$$\gamma \approx 2.66. \tag{4.7}$$

Algebraic decay of the Poincaré recurrences was observed in many Hamiltonian flows and area-preserving maps [63,62]. Its connection with anomalous transport was established in Ref. [63].

To find an origin of long recurrences in our system, we want to know, ‘‘where in the phase space the tracer travels during such long excursions?’’ To get a direct answer to this question, we have plotted long Poincaré cycles, color coding them by their recurrence times (Fig. 10). Poincaré cycle C_i is a piece of an orbit of the map $\hat{M}$ between two successive returns: $C_i = \{z_n : n_i \leq n < n_{i+1}\}$. In Fig. 10 only cycles longer than $N_{\min} = 500$ map periods ($\tau_i > N_{\min} T_{\text{tel}} \approx 10^4$) are included. One can see, that the distribution of the orbit points in the phase space is highly nonuniform, they are concentrated around the regular islands and in the thin layer on the outer boundary of the mixing region, in other words, in the neighborhood of every KAM surface, bordering the stochastic sea. This is a manifestation of the well-known effect of the stickiness of the KAM surfaces (see for example, Ref. [59]). The deeper the particle penetrates into the hierarchical structure on the island border, the longer time it is trapped there. Color coding in Fig. 10 illustrates this effect: longest cycles (red) are those, which got closest to the island border.

Trapping of the tracers in the sticky *singular zones* on the borders of the chaotic region seems to be the only mechanism causing the long-term correlations in our system. Qualitatively, the stickiness of KAM surfaces is caused by the fact, that effective Lyapunov exponents in the vicinity of islands are vanishingly small. One of the first models attempting to explain the way quasitraps work, introduced a diffusion coefficient, continuously approaching zero as the distance from the trajectory to the boundary KAM surface tends to zero [64]. Recently, a similar mechanism was found to be responsible for anomalous longtitudal dispersion in temporally irregular transversely bounded shear flow [32]. But for periodically perturbed Hamiltonian systems, in contrast to this ‘‘smooth escape’’ mechanism, numerical experiments show, that particle escapes from the trap in a series of jumps, as the trajectory suddenly crosses partial barriers (cantori) stratifying the phase space near regular islands. This give rise to Markov chain and Markov tree models [65] [26], which describe the quasidiscrete nature of transport in terms of fluxes through individual cantori, organized in a self-similar pattern, assuming that between two consecutive crossings particle moves in a random manner for long enough time to lose memory. Figure 11 shows the character of particle escape from a singular zone around one of the vortex cores in our system. We have put two tracers close to the core boundary, and followed the distance from them to the central vortex. Initially it oscillates between two values–tracers are trapped between two oval cantori, with well-defined borders. Then, suddenly, a tracer hits a hole in a cantorus, and jumps to another ‘‘level,’’ where it gets stuck again, bounded to stay inside by another barrier. Sooner or later it finds a hole in that one, too, and eventually escapes into the chaotic sea.

Figure 10 shows, that several traps contribute to the algebraic flight tail of Poincaré recurrences PDF, and that these traps considerably differ in size, shape, and structure. To

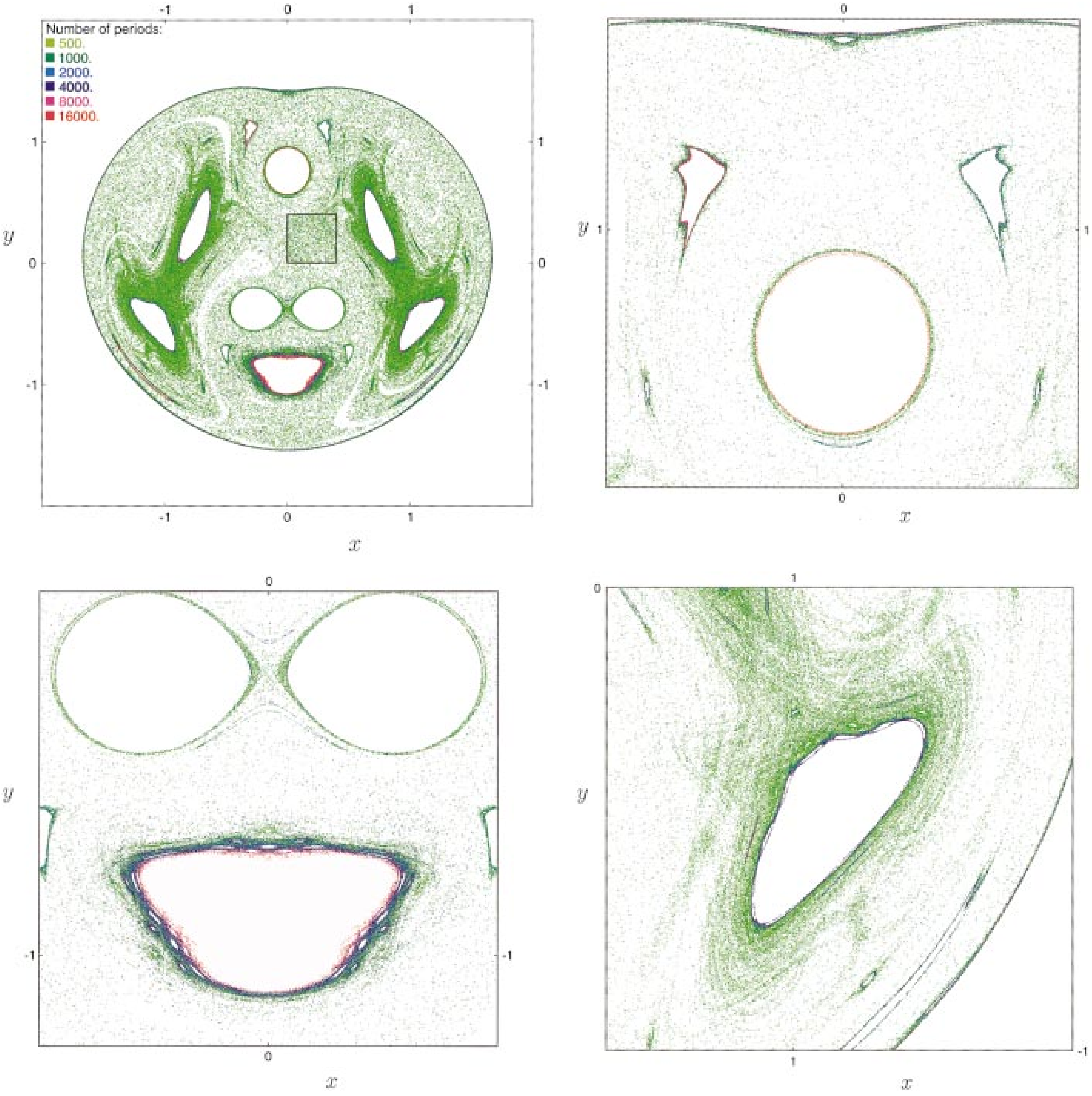

FIG. 10. (Color) Poincaré cycles, color-coded according to their recurrence time, measured in number of periods of relative vortex motion $T_{\rm rel}=19.57$. Longest cycles are concentrated in singular sticky zones near KAM islands.

compare their relative effects, let us define the PDF of the *residence time* (or stickiness time—time spent in a particular trap) $P_{Q_i}(t)$ for each trap Q_i. To determine $P_{Q_i}(t)$, we need to specify trap boundaries ∂Q_i, however, tails of residence time distribution practically do not depend on the exact position of ∂Q_i, as long as all singular zones (inside which the tracer spends most of the trapping time) belonging to a given trap are completely inside it. In our system individual traps are well separated from each other by a chaotic sea, and appropriate boundaries can be easily chosen to define trap domains. We have analyzed the following traps: $Q_1: x \in (-0.36,0.36)$, $y \in (-1.2,-0.5)$ (big island in the bottom of Fig. 10); $Q_2: x \in (0.5,1)$, $y \in (-0.2,0.9)$ (one of the four big side islands); $Q_3: x \in (0.2,0.4)$, $y \in (0.9,1.2)$ (one of the four small islands close to the outer border); $Q_4: x^2+y^2 > 1.3^2$ (outer rim of the chaotic sea). All distributions are extracted from the same set of trajectories, and normalized on a total number of trappings in that particular domain.

Our approach in determining residence time statistics differs from the conventional one, based on the measurement of *exit time* distributions $P_e(t)$, by initializing many particles inside the trap and finding the probability density of escape by counting particles leaving the trap. Exit time measurements allow to collect a very good statistics and thus reach high accuracy in determining $P_e(t)$ [27,37]. However, exit time distributions are defined for each sticky zone individu-

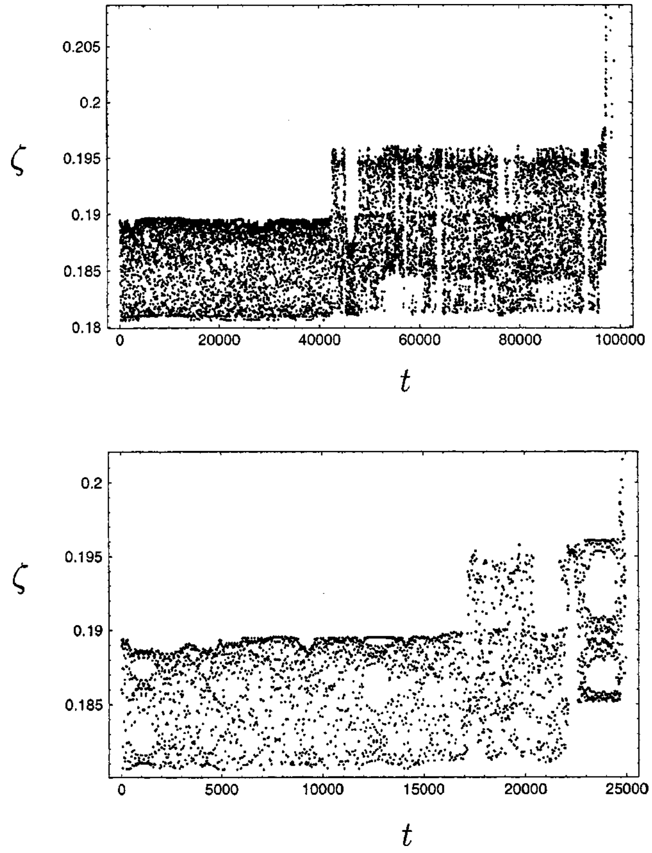

FIG. 11. Two examples of escape from the sticky band around vortex core. Distance from the central vortex to the tracer ζ vs time is shown.

ally, and cannot be used to compare different traps. Roughly speaking, $P_e(t)$ tells us how sticky the singular zone is, but does not tell how big it is. When we initialize a particle randomly in the chaotic sea, and analyze all the flights it experiences on the way, we can characterize the size of each trap by the frequency with which it is visited. Implementation of these procedure is computationally expensive, since a particle can wander for a long time without visiting any trap, but the necessary data can be collected from the same ensemble we have used for the transport simulations at minimal increase in the computation cost.

Tails of the residence times PDF for the traps Q_i, defined above, are shown in Fig. 12. The decay of $P_{Q_i}(t)$ at large times is algebraic:

$$P_{Q_i}(t)=A_i t^{-\gamma_i} \tag{4.8}$$

with approximately the same value of the decay exponent for all four traps

$$\gamma_i \approx 2.5. \tag{4.9}$$

Whether all the exponents γ_i should be *exactly* the same, i.e., whether the value of the decay exponent in the Hamiltonian systems is universal or not, is a question with a long history (see for example, Refs. [62] and [66]), and its discussion is not in the scope of the present paper. We will only note, that our exponents, coming from the traps with considerably different geometry, are nevertheless close enough to each other, so that on the scale of simulation time ($t_{\max} \approx 5\times 10^5$) the relative effect of the traps are determined by the values of the tail strengths A_i, rather than by the differences in γ_i. As can be seen from Fig. 11, there is no single dominating trap—the big trap around the bottom island Q_1, the trap around the four big islands on the side Q_2, and the outside rim trap Q_4 have approximately the same strength, and the smaller trap Q_3 has strength about five times less than that. The value for the Poincaré recurrence exponent (4.7) agrees reasonably well with the stickiness exponent (4.9), as should be expected. In summary, we may say that the flight tail of the Poincaré recurrences PDF is determined by the cumulative effect of trappings in several singular zones with similar power-law large-time asymptotic of the residence time distribution.

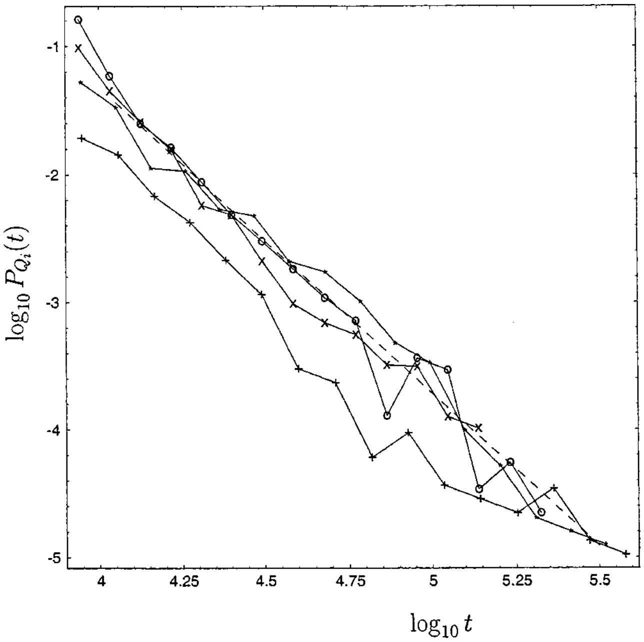

FIG. 12. Tails of residence time distributions for the traps Q_i (defined in the text). All four distributions are obtained from the same tracer ensemble, so that relative importance of each trap can be seen. Average decay exponent (slope of the linear fit) is $\gamma_i = 2.5$.

The effect of a singular zone on transport depends not only on its residence time PDF, but also on how fast the tracer is moving when it is trapped. The average rotation frequency of tracers in the trap around a KAM island is very close to the rotation frequency of the island itself, provided the center of vorticity always stays outside of the island. The latter depends on the way the island is advected during one period of vortex relative motion T_{rel}. From phase portraits in Fig. 4, we can obtain

$$\nu_1=\nu_{\text{rot}}+\nu_{\text{rel}}=0.138; \quad \nu_{2,3}=\nu_{\text{rot}}-1/2\nu_{\text{rel}}=0.0626 \tag{4.10}$$

for the island in Q_1, Q_2, Q_3. Comparing ν_i with the average tracer angular advection frequency $\overline{\nu}=0.0742$ (3.2), we see, that Q_1 is producing fast flights, rotating forward with $\Delta\nu_1 = \nu_1 - \overline{\nu} = 0.0638$ relative to the chaotic background, while Q_2 and Q_3 are slow traps, rotating backward with respect to the background with frequency $\Delta\nu_{2,3}=\nu_{2,3}-\overline{\nu}=-0.0116$.

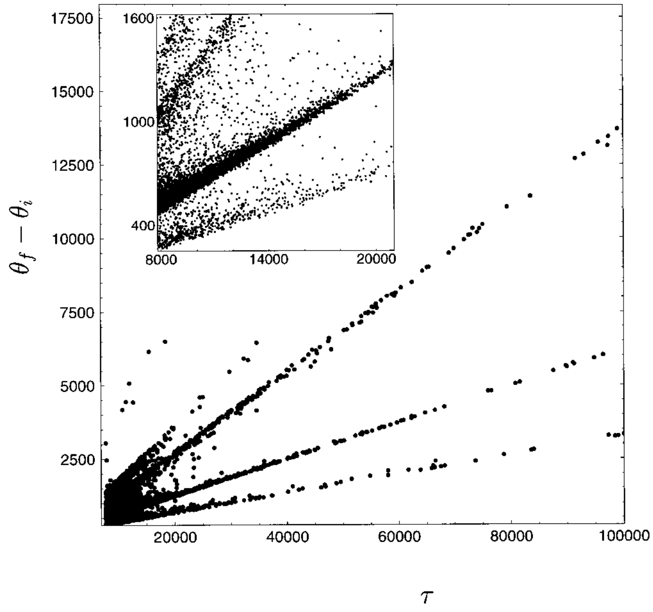

FIG. 13. Scatter plot of flight lengths (net angle covered during the cycle, $\theta_f - \theta_i$) versus trapping time τ.

Note, that $\Delta \nu_1$ is six times larger than $\Delta \nu_{2,3}$, so that the influence of fast trappings on the angular PDF of the tracer $P(\theta,t)$ should be stronger. The asymmetry of $P(\theta,t)$ confirms this suggestion—the right (fast) tail in Fig. 6(a) is much more pronounced than the left (slow) one.

Another way of looking at long-time cycles is to analyze how fast tracers rotate during that time. Figure 13 shows a scatter plot of a net angle, covered by a tracer, $\theta_f - \theta_i = \theta(n_i T_{\mathrm{rel}}) - \theta(n_{i-1} T_{\mathrm{rel}})$ versus recurrence time τ_i. All cycles, longer than 50 000 lie on one of the three straight lines, corresponding to the angular frequencies of the above mentioned islands: $\nu_1 \approx 0.138$, $\nu_{2,3} \approx 0.0626$, and to the angular frequency of a tracer trapped in the outer rim trap Q_4: $\nu_4 \approx 0.032$. On shorter time scale, $\tau \approx 10^4$, the majority of the cycles are still clustered along these lines, but a whole bunch of cycles with random average frequency appear. They correspond to trajectories, which were stuck to two or more different traps on their way between successive returns to B. The dominance of one-flight recurrences can be explained by comparing probabilities of having a recurrence in a given time t due to one-trap and two-trap flights. If a one-trap probability is given by a power law (for large t): $P_1(t) \sim t^{-\gamma}$, then two-trap probability decays as:

$$P_2(t) \sim \int_0^t \tau^{-\gamma}(t-\tau)^{-\gamma} d\tau \sim t^{-2\gamma+1}, \qquad (4.11)$$

i.e., faster than $P_1(t)$ for $\gamma > 1$. The latter inequality always holds for Hamiltonian systems, due to the existence of the mean recurrence time: integral in Eq. (4.3) must converge.

V. SUMMARY AND CONCLUSION

Analysis of the advection in the flow field of three identical point vortices, performed in this paper, reveals a number of features, which can be relevant in case of more general two-dimensional (2D) incompressible flows, and particularly in multivortex systems. The case of three-vortex flow is special—it is one of the simplest systems generating Lagrangian chaos. Motion of the vortices, specifying the flow, is governed by a Hamiltonian system, which turns out to be integrable due to the sufficient number of independent conservation laws. Advection equation, written in a reference frame corotating with vortices, has a structure of a periodically forced Hamiltonian system, which allows to carry out its detailed analytical and numerical study, using well-developed methods for $1\frac{1}{2}$ degrees of freedom Hamiltonian systems.

The phase space (advection plane) of a passive particle in a three-vortex flow contains a variety of structures, that influences tracer motion in the chaotic sea. These structures are responsible for intermittent character of a chaotic tracer trajectory; a tracer, being trapped in the hierarchy of cantori in the neighborhood of an regular island, moves in an almost quasiperiodic manner, closely imitating a KAM trajectory. Occurrence of such long ballistic flights leads to anomalous (superdiffusive) transport properties of chaotic motion. Scaling exponent, describing the behavior of central part of tracer distribution and low noninteger moments differs from the transport exponent in the power law for the growth of variance, which indicates, that we are dealing with a case of strong anomalous diffusion [45]. The shape of the azimuthal tracer distribution is non-Gaussian: it is asymmetric and has long tails. Similar distributions were observed in a model of vortices in shear [36].

Anomalous transport in Hamiltonian systems typically implies non-Poissonian character of Poincaré recurrences distribution [63,58]; in accordance with this relation, Poincaré cycle distribution in three-vortex flow exhibits power-law decay for large recurrence times. Analysis of long correlations shows that they are caused by sticking of tracers to the boundaries of KAM islands inside the mixing region and to the outer border of the chaotic sea. Long Poincaré cycles are concentrated in the singular zones (quasitraps) and can be used to detect the relevant ones, i.e., those, that produce strong stickiness, and visualize their structure. Residence time distributions of several major traps have approximately the same value of decay exponent, and their contributions to transport anomalies are comparable. The principal traps are of different shape, structure and origin, and rotation frequencies of corresponding flights are not the same: some flights move faster than the background, and some slower. To reproduce observed asymmetric distributions, a stochastic model of tracer advection should incorporate the effect of competing flights with different velocities.

In conclusion, we would like to point out, that the present work should be considered not only as a study of mixing properties in a rather particular velocity filed, but also as a nontrivial example of anomalous transport in dynamical systems. Advection in a three-vortex flow provides an important link between abstract models of modern dynamical system theory, and much more complicated models of particle advection in hydrodynamic flows. New techniques, developed and tested here, such as locating sticky zones via analysis of Poincaré recurrences, can be useful in the studies of passive particle transport in harder problems of geophysical fluid dynamics, such as pollution dispersion in the atmosphere and ocean, ozone transport in the Antarctic polar vortex, large-scale mixing in the ocean, etc.

ACKNOWLEDGMENTS

We would like to thank S. Boatto for providing the results of their work prior to publication. This work was supported by the US Department of Navy, Grant No. N00014-96-1-0055, and the US Department of Energy, Grant No. DE-FG02-92ER54184. We thank NPACI for providing computer time on the SP2 machine at the University of Michigan.

[1] H. Aref, Philos. Trans. R. Soc. London, Ser. A **333**, 273 (1990).
[2] J. Ottino, *The Kinematics of Mixing: Stretching, Chaos, and Transport* (Cambridge University Press, Cambridge, 1989).
[3] J. Ottino, Annu. Rev. Fluid Mech. **22**, 207 (1990).
[4] V. Rom-Kedar, A. Leonard, and S. Wiggins, J. Fluid Mech. **214**, 347 (1990).
[5] A. Crisanti, M. Falcioni, G. Paladin, and A. Vulpiani, Nuovo Cimento **14**, 1 (1991).
[6] A. Crisanti, M. Falcioni, A. Provenzale, P. Tanga, and A. Vulpiani, Phys. Fluids A **4**, 1805 (1992).
[7] G. Haller and A. Poje, Physica D **119**, 352 (1998).
[8] P. D. Miller, C. K. R. T. Jones, A. M. Rogerson, and L. J. Pratt, Physica D **101**, 1 (1997).
[9] L. Kuznetsov and G. M. Zaslavsky, Phys. Rev. E **58**, 7330 (1998).
[10] S. L. Ziglin, Dokl. Adad. Nuak SSSR **250**, 1256 (1980) [Sov. Math. Dokl. **21**, 296 (1980)].
[11] H. Aref and N. Pomphrey, Phys. Lett. A **78**, 297 (1980).
[12] H. Aref, J. Fluid Mech. **143**, 1 (1984).
[13] N. J. Zabusky and J. C. McWilliams, Phys. Fluids **25**, 2175 (1982).
[14] A. Babiano, G. Boffetta, A. Provenzale, and A. Vulpiani, Phys. Fluids **6**, 2465 (1994).
[15] O. U. Velasco Fuentes, G. J. F. van Heijst, and N. P. M. van Lipzig, J. Fluid Mech. **307**, 11 (1996).
[16] P. W. C. Vobseek, J. H. G. M. van Geffen, V. V. Meleshko, and G. J. F. van Heijst, Phys. Fluids **9**, 3315 (1997).
[17] Z. Neufeld and T. Tél, J. Phys. A: Math. Gen. **30**, 2263 (1997).
[18] Á. Péntek, T. Tél, and Z. Toroczkai, J. Phys. A: Math. Gen. **28**, 2191 (1995).
[19] Y. Kimura and H. Hasimoto, J. Phys. Soc. Jpn. **55**, 5 (1986).
[20] L. Zannetti and P. Franzese, Eur. J. Mech. B/Fluids **12**, 43 (1993).
[21] G. Boffetta, A. Celani, and P. Franzese, J. Phys. A: Math. Gen. **29**, 3749 (1996).
[22] H. Aref and M. A. Stremler, J. Fluid Mech. **314**, 1 (1996).
[23] S. Boatto and R. T. Pierrehumbert, J. Fluid Mech. **394**, 137 (1999).
[24] Z. Neufeld and T. Tél, Phys. Rev. E **57**, 2832 (1998).
[25] M. F. Shlesinger, G. M. Zaslavsky, and J. Klafter, Nature (London) **363**, 31 (1993).
[26] J. D. Meiss and E. Ott, Physica D **20**, 387 (1986).
[27] G. M. Zaslavsky, M. Edelman, and B. A. Niyazov, Chaos **7**, 159 (1997).
[28] B. V. Chirikov, Phys. Rep. **52**, 264 (1979).
[29] A. B. Rechester and R. White, Phys. Rev. Lett. **44**, 1586 (1980).
[30] T. H. Solomon, E. R. Weeks, and H. L. Swinney, Physica D **76**, 70 (1994).
[31] E. R. Weeks, J. S. Urbach, and H. L. Swinney, Physica D **97**, 219 (1996).
[32] S. C. Venkataramani, T. M. Antonsen, Jr., and E. Ott, Physica D **112**, 412 (1998).
[33] R. Ramshankhar, D. Berlin, and J. Gollub, Phys. Fluids A **2**, 1955 (1990).
[34] O. Cardoso and P. Tabeling, Europhys. Lett. **7**, 225 (1988).
[35] P. Tabeling, A. E. Hansen, and J. Paret, in ‘‘*Chaos, Kinetics and Nonlinear Dynamics in Fluids and Plasmas*,’’ edited by S. Benkadda and G. Zaslavsky (Springer, Berlin, 1998), p. 145.
[36] D. del-Castillo-Negrete, Phys. Fluids **10**, 576 (1998).
[37] G. M. Zaslavsky and M. Edelman, Phys. Rev. E **56**, 5310 (1997).
[38] S. Benkadda, S. Kassibrakis, R. B. White, and G. M. Zaslavsky, Phys. Rev. E **55**, 4909 (1997).
[39] E. W. Montroll and M. F. Shlesinger, in *Studies in Statistical Mechanics*, edited by J. Lebowtiz and E. Montroll (North-Holland, Amsterdam, 1984), Vol. 11, p. 1.
[40] M. F. Shlesinger, B. J. West, and J. Klafter, Phys. Rev. Lett. **59**, 1100 (1987).
[41] T. Geizel, A. Zacherl, and G. Randons, Phys. Rev. Lett. **59**, 2503 (1987).
[42] T. Geizel, A. Zacherl, and G. Radons, Z. Phys. B: Condens. Matter **71**, 117 (1988).
[43] G. M. Zaslavsky, in *Topological Aspects of the Dynamics of Fluids and Plasmas*, edited by H. K. Moffatt *et al.* (Kluwer, Dordrecht, 1992), p. 481; Chaos **4**, 25 (1994); Physica D **76**, 110 (1994).
[44] A. I. Saichev and G. M. Zaslavsky, Chaos **7**, 753 (1997).
[45] P. Castiglione, A. Mazzino, P. Muratore-Ginanneschi, and A. Vulpiani, e-print chao-dyn/9811012 (1998).
[46] K. O. Friedrichs, *Special Topics in Fluid Dynamics* (Gordon and Breach, New York, 1966).
[47] E. A. Novikov Zh. Eksp. Teor. Fiz. **54**, 1590 (1968) [Sov. Phys. JETP **41**, 937 (1975)].
[48] H. Aref, Phys. Fluids **22**, 393 (1979).
[49] J. L. Synge, Can. J. Math. **1**, 257 (1949).
[50] J. Tavantzis and L. Ting, Phys. Fluids **31**, 1392 (1988).
[51] V. V. Meleshko and M. Yu. Konstantinov, *Vortex Dynamics and Chaotic Phenomena* (World Scientific, Singapore, 1999).
[52] Y. Kimura, J. Phys. Soc. Jpn. **56**, 2024 (1987).
[53] Y. Kimura, Physica D **46**, 439 (1990).
[54] V. V. Melezhko, M. Yu. Konstantinov, A. A. Gurzhi, and T. P. Konovaljuk, Phys. Fluids A **4**, 2779 (1992).
[55] R. I. McLachlan and P. Atela, Nonlinearity **5**, 541 (1992).
[56] D. I. Pullin and P. G. Saffman, Proc. R. Soc. London, Ser. A **432**, 481 (1991).
[57] S. Benkadda, S. Kassibrakis, R. B. White, and G. M. Zaslavsky, Phys. Rev. E **59**, 3761 (1999).
[58] G. M. Zaslavsky, D. Stevens, and H. Weitzner, Phys. Rev. E **48**, 1683 (1993).
[59] G. M. Zaslavsky, *Physics of Chaos in Hamiltonian Systems* (Imperial College Press, London, 1998).
[60] M. Kac, *Probability and Related Topics in Physical Sciences*,

Boulder, Colorado, 1957 (Wiley Interscience, New York, 1958).

[61] J. D. Meiss, Chaos **7**, 139 (1997).

[62] B. V. Chirikov and D. L. Shepelyansky, Physica D **13**, 395 (1984).

[63] G. M. Zaslavsky and M. K. Tippett, Phys. Rev. Lett. **67**, 3251 (1991).

[64] B. V. Chirikov, in *Lecture Notes in Physics Vol. 179*, (Springer, New York, 1983), p. 29.

[65] J. D. Hanson, J. R. Cary, and J. D. Meiss, J. Stat. Phys. **39**, 327 (1985).

[66] Y. C. Lai, M. Ding, C. Grebodi, and R. Blumel, Phys. Rev. A **46**, 4661 (1992).